

Optical Mapping Approaches on Muscleblind-Like Compound Knockout Mice for Understanding Mechanistic Insights Into Ventricular Arrhythmias in Myotonic Dystrophy

Chung-Chuan Chou, MD;* Po-Cheng Chang, MD;* Yi-Chia Wei, MD; Kuang-Yung Lee, MD, PhD

Background—Cardiac arrhythmias are common causes of death in patients with myotonic dystrophy (dystrophia myotonica [DM]). Evidence shows that atrial tachyarrhythmia is an independent risk factor for sudden death; however, the relationship is unclear.

Methods and Results—Control wild-type ($Mbnl1^{+/+}; Mbnl2^{+/+}$) and DM mutant ($Mbnl1^{-/-}; Mbnl2^{+/-}$) mice were generated by crossing double heterozygous knockout ($Mbnl1^{+/-}; Mbnl2^{+/-}$) mice. In vivo electrophysiological study and optical mapping technique were performed to investigate mechanisms of ventricular tachyarrhythmias. Transmission electron microscopy scanning was performed for myocardium ultrastructural analysis. DM mutant mice were more vulnerable to anesthesia medications and program electrical pacing: 2 of 12 mice had sudden apnea and cardiac arrest during premedication of general anesthesia; 9 of the remaining 10 had atrial tachycardia and/or atrioventricular block, but none of the wild-type mice had spontaneous arrhythmias; and 9 of 10 mice had pacing-induced ventricular tachyarrhythmias, but only 1 of 14 of the wild-type mice. Optical mapping studies revealed prolonged action potential duration, slower conduction velocity, and steeper conduction velocity restitution curves in the DM mutant mice than in the wild-type group. Spatially discordant alternans was more easily inducible in DM mutant than wild-type mice. Transmission electron microscopy showed disarranged myofibrils with enlarged vacuole-occupying mitochondria in the DM mutant group.

Conclusions—This DM mutant mouse model presented with clinical myofibril ultrastructural abnormality and cardiac arrhythmias, including atrial tachyarrhythmias, atrioventricular block, and ventricular tachyarrhythmias. Optical mapping studies revealed prolonged action potential duration and slow conduction velocity in the DM mice, leading to vulnerability of spatially discordant alternans and ventricular arrhythmia induction to pacing. (*J Am Heart Assoc.* 2017;6:e005191. DOI: 10.1161/JAHA.116.005191.)

Key Words: conduction block • *Mbnl* knockout mice • myotonic dystrophy • optical mapping • ventricular tachyarrhythmias

Myotonic dystrophy (dystrophia myotonica [DM]) is an autosomal dominant disorder characterized by progressive skeletal muscle weakness, myotonia, and

multisystemic features. DM type I (DM1) is the more severe type of DM that is caused by unstable microsatellite (CTG)_n expansion (n>50) in the 3' untranslated region of the *DMPK* gene.¹ DM type II is a milder form that is caused by (CCTG)_n expansion (n>75) in the first intron of the *CNBP* gene.² Arrhythmia is the second most common cause of death for patients with DM1, only after respiratory failure.^{3,4} Similar to skeletal muscle, the length of (CTG)_n expansion correlates with the severity of cardiac manifestations in most series.^{5,6} While heart failure is found only in end-stage DM patients, conduction block is more common and ranges from asymptomatic first-degree atrioventricular block to severe Stokes-Adams attack in early-stage DM patients. The ECG and electrophysiological findings include prolongation of the PR interval, increased QRS complex duration, and prolongation of the His-ventricular interval.⁷ Of note, signs of conduction block are associated with developing lethal ventricular tachycardia/fibrillation (VT/VF). DM patients who have a family history of sudden death or who are older than 40 years

From the Department of Cardiology, Chang Gung Memorial Hospital, Linkou, Taiwan (C.-C.C., P.-C.C.); Department of Neurology, Chang Gung Memorial Hospital, Keelung, Taiwan (Y.-C.W., K.-Y.L.); College of Medicine, Chang Gung University, Taoyuan, Taiwan (C.-C.C., P.-C.C., K.-Y.L.).

An accompanying Video S1 is available at <http://jaha.ahajournals.org/content/6/4/e005191/DC1/embed/inline-supplementary-material-1.avi>

*Dr Chou and Dr Chang contributed equally to this work.

This work was presented in part at the American Heart Association Scientific Sessions, November 7–11, 2015, in Orlando, FL.

Correspondence to: Kuang-Yung Lee, MD, PhD, No. 222, Mai-Chin Rd, Keelung 204, Taiwan. E-mails: kylee@cgmh.org.tw, moritakaky@yahoo.com
Received November 29, 2016; accepted March 15, 2017.

© 2017 The Authors. Published on behalf of the American Heart Association, Inc., by Wiley. This is an open access article under the terms of the Creative Commons Attribution-NonCommercial License, which permits use, distribution and reproduction in any medium, provided the original work is properly cited and is not used for commercial purposes.

appear to have higher risk^{5,8}; however, adolescent patients with increases in heart rate during physical exercise may also experience sudden cardiac death.⁹ Although severe ECG abnormalities that are indicative of conduction block and sustained atrial tachyarrhythmias (eg, atrial fibrillation) could be independent risk factors for sudden death,⁷ the relationship between atrial arrhythmia-conduction abnormality and ventricular arrhythmias remains unclear. This evidence implies that rate-dependent factors and ventricular conduction abnormalities play a role in ventricular arrhythmogenesis in DM patients. Although prophylactic permanent pacemaker implantation may reduce the incidence of sudden cardiac death in DM patients,¹⁰ sudden death caused by ventricular tachyarrhythmias still occurs in these patients, suggesting that ventricular tachyarrhythmias may be more frequent than expected.^{7,11} Therefore, an implantable cardioverter-defibrillator that is capable of both pacing and defibrillation is recommended for patients at high risk for ventricular tachyarrhythmias. In recent series, relatively high incidences (14.3–33.3%) of ventricular tachycardia in patients with implantable cardioverter-defibrillator implantation were observed and shocks were appropriately provided.^{12,13}

Accumulating evidence shows that pathogenic RNA could generate toxic effects throughout the sequestration and, subsequently, loss of function of muscleblind-like (MBNL) proteins. The MBNL family consists of 3 members (MBNL1, MBNL2, and MBNL3) and they are RNA-binding proteins critical for splicing regulations and polyadenylations during the developmental transition from fetal to adult.^{14–17} *Mbnl1* knockout (KO) mice recapitulate myotonia and skeletal muscle pathology,¹⁸ and *Mbnl2* KO mice reproduce abnormal sleep pattern and cognitive decline.¹⁹ While *Mbnl1*^{-/-}; *Mbnl2*^{-/-} double KOs are embryonic lethal, *Mbnl1*^{-/-}; *Mbnl2*^{+/-} (*Mbnl1* KO; *Mbnl2* heterozygous [HET]) mice show enhanced myotonia and cardiac abnormalities including conduction block, dilated cardiomyopathy, focal fibrosis, and sudden death.²⁰ Although these mice showed reduced life span, there was no direct evidence for verifying the mechanisms of sudden death. In this study, we conducted simultaneously monitored intracellular calcium (Ca_i) and membrane voltage (V_m) mapping on *Mbnl1* KO; *Mbnl2* HET mice to investigate possible mechanisms of ventricular tachyarrhythmias.

Materials and Methods

Mbnl Compound KO Mouse Model

Original articles describing the generation of *Mbnl1* and *Mbnl2* single KOs,^{18,19} as well as *Mbnl1* KO; *Mbnl2* HET compound KO mice, have been published.²⁰ For current experiments, the *Mbnl1* KO; *Mbnl2* HET (DM mutant) mice were generated by crossing 2 single KO lines in the animal center of Chang Gung

Memorial Hospital, Keelung, Taiwan, which is an AAALAC-accredited institute conducting appropriate breeding and experiments for biomedical research that meet the standards of animal welfare. The siblings with *Mbnl1*^{+/+}; *Mbnl2*^{+/+} were used as the wild-type (WT) control group. All experimental procedures were approved by the Institutional Animal Care and Use Committee (IACUC) at Chang Gung Memorial Hospital, Keelung (IACUC No. 2014020501) and Linkou (IACUC No. 2015111001), Taiwan. All of the mice used in this study were 2 to 4 months of age, due to a reduced life expectancy (no more than 6 months) in this compound KO line. In total, 16 DM mutant and 18 WT control mice were used.

In Vivo Electrophysiological Study and Langendorff Heart Preparation

Mice were premedicated with xylazine (10 mg/kg IP) and zoletil (25 mg/kg IP), and anesthetized with isoflurane 1.0% to 2.0% in an anesthesia chamber. When the mice were fully anesthetized and unresponsive to physical stimuli, endotracheal intubation was performed for gas general anesthesia (isoflurane 0.5–1%) and the chests were opened via a median thoracotomy to expose the heart. To perform surface electrocardiography, electrodes were attached to limbs, and 3-lead electrocardiography was performed with Axon Digidata (Molecular Devices, CA, USA) to record the PR interval and arrhythmias in vivo for 5 to 10 minutes. The hearts were then excised and rinsed in Tyrode's solution (in mmol/L: NaCl 125, KCl 4.5, NaH₂PO₄ 1.8, NaHCO₃ 24, CaCl₂ 0.9, MgCl₂ 0.5, and glucose 5.5 in deionized water), cannulated via ascending aorta with a 20-gauge stainless steel blunt needle and perfused at a flow rate of 1.5 to 3 mL/min to keep the average perfusion pressure around 80 cmH₂O on a Langendorff apparatus with warm (37°C) oxygenated Tyrode's solution, which was bubbled with 95% O₂/5% CO₂ to maintain a pH of 7.40±0.05. The hearts were immersed in a temperature-controlled tissue bath and maintained at 37°C. Pseudo-ECG recordings were obtained using 3 spaced electrodes located in the bath surrounding the hearts.

Optical Mapping Studies

Dual optical mapping techniques were used to study the anterior aspect of the hearts. Calcium indicator Rhod-2AM (5 μmol/L, dissolved in dimethyl sulfoxide via mixing with pluronic F-127; Molecular Probes, OR, USA) and voltage indicator RH237 (1 μmol/L in 20 mL Tyrode's solution, dissolved in dimethyl sulfoxide; Molecular Probes) were used for Ca_i and V_m staining, respectively. Blebbistatin (15 μmol/L; Tocris Bioscience, Minneapolis, MN, USA) was added to the Tyrode's solution to reduce motion artifacts. The hearts were illuminated with a solid-state, frequency-doubled laser

(Millennia, Spectra-Physics Inc, Newport Corporation, Irvine, CA, USA) at a wavelength of 532 nm. Epifluorescence was collected simultaneously through 2 high-speed cameras (MiCAM Ultima, BrainVision, Tokyo, Japan) at 1 ms per frame through a 580 ± 20 -nm bandpass filter and a 715-nm long-pass filter for Ca_i and V_m images, respectively. Digital images (100×100 pixels) were gathered from the epicardium of the mapped ventricles (14×14 mm² area), resulting in a spatial resolution of 140×140 μm^2 per pixel. Baseline fluorescence level (\bar{F}) of an individual pixel was first calculated for the duration of recording. The ratio of fluorescence ($F - \bar{F}/\bar{F}$) of an individual pixel was processed with both spatial (3×3 pixels Gaussian filter) and temporal (3 frames moving average) filtering to generate the maps. A bipolar lead was used to pace the lateral wall of the left ventricle at a double threshold. The effective refractory period was measured by giving a premature stimulus after 8 beats at a 200-ms pacing cycle length (PCL). Arrhythmogenic alternans and conduction velocity (CV) were studied using a dynamic pacing protocol: decremental pacing at a PCL of 200 ms, then decreased in 10-ms steps until loss of 1:1 capture or induction of ventricular tachyarrhythmias. Ventricular tachyarrhythmia inducibility was defined as the ability to provoke VT/VF with the dynamic pacing protocol and/or programmed extra stimuli (up to 4 premature stimuli). Sustained ventricular arrhythmia was defined as duration longer than 30 seconds.

Transmission Electron Microscopy of Cardiac Muscles

The mice were anesthetized and the hearts were harvested by thoracotomy. Primary fixation of cardiac muscle samples from the left ventricles were performed with 3% glutaraldehyde and 2% paraformaldehyde in 0.1 mol/L sodium cacodylate buffer for 1 hour at 4°C. Secondary fixation was performed with 1% osmium tetroxide in 0.1 mol/L cacodylate buffer at 4°C for 1 hour and followed by washing. For imparting additional contrast and further fixation, immersion using 2% uranyl acetate for 2 hours in a dark room was performed. The tissues were then dehydrated with a graded series of ethanol and immersed in a transient solvent of 100% propylene oxide. Specimens were embedded with a gradient infiltration of propylene oxide: Epon resin, followed by 100% resin under vacuum. Tissue blocks were sectioned into 75 nm thickness with ultramicrotome for examination under Hitachi H-7500 transmission electron microscopy (Hitachi Ltd, Tokyo, Japan).

Immunoblotting

For protein extraction, the hearts were dissected and homogenized with CelLytic MT cell lysis reagent (Sigma-Aldrich), followed by sonication and centrifugation. The protein

concentrations were determined by protein assay (Bio-Rad) and equal amounts (50 μg) of extracted proteins were loaded for analysis. The samples were resolved by 8% SDS-PAGE and wet-transferred to a polyvinylidene difluoride membrane overnight. The proteins were detected by immunoblotting using mouse monoclonal antibody anti-Actin (Merck Millipore) and rabbit polyclonal antibody anti-SCN5A (Aviva Systems Biology) as well as horseradish peroxidase-conjugated anti-mouse or anti-rabbit secondary antibody (Thermo Fisher Scientific) followed by chemiluminescent detection with Immobilon Western HRP Substrate (Merck Millipore).

Data Analysis

Action potential duration (APD) was measured from 20% depolarization to 80% repolarization (APD_{80}) at PCLs of 200, 150, 120, and 100 ms. Ca_i transient duration (Ca_iTD_{80}) was measured by the same method.²¹ APD_{80} and Ca_iTD_{80} dispersion represent the SD of all available APD_{80} and Ca_iTD_{80} data at PCLs of 200, 150, 120, and 100 ms. We plotted APD restitution graphs of APD_{80} versus the preceding diastolic interval, defined as the interval between 80% repolarization and the onset of the next action potential, as previously described.²² The curves of APD restitution were constructed by polynomial fitting, and the steepest slopes of APD restitution curves were calculated at the diastolic interval. We used monoexponential fitting to compute time constant (τ) of the decay portion of the Ca^{2+} transient at a PCL of 200 ms. V_m and Ca_i alternans were defined as the differences in APD_{80} of 2 consecutive beats >4 ms and in Ca_i transient amplitude of 2 consecutive beats $>10\%$. The phase was defined as positive for a short-long APD_{80} and a small-large Ca_i amplitude sequence (color coded by red) and as negative for a long-short APD_{80} and a large-small Ca_i amplitude sequence (color coded by green). Spatially discordant alternans (SDA) was evidenced by the presence of both red and green regions separated by a nodal line. To estimate CV, we measured the distance and conduction time between the earliest activation point and 2 epicardial points: one was from the pacing site to the left ventricular apex, and the other was along an axis parallel to the atrioventricular ring at PCLs of 200, 150, 120, 100, 90, 80, and 70 ms. When CV alternans occurred, we selected the slower ones for comparisons. We plotted CV restitution graphs of CV versus the preceding diastolic interval. The steepest curves of CV restitution graphs were constructed by polynomial fitting, and the slope of CV restitution curve was calculated at the shortest diastolic interval.

Statistical Analysis

Continuous variables are shown in mean \pm SD values and categorical variables are presented as absolute numbers and percentages. Unpaired Student *t* test was performed for

comparison between 2 groups. For the statistical comparisons of ventricular tachyarrhythmia inducibility, Fisher exact test was used. The Wilcoxon rank sum test was used to compare protein expression between the 2 groups. Statistical analyses were performed using SPSS statistical software for Windows version 22 (IBM Corp, Armonk, NY). A $P < 0.05$ was considered statistically significant.

Results

Twelve DM mutant mice (mean age 144 ± 39 days) and 14 WT mice (mean age 158 ± 52 days) ($P = 0.47$) were included in the electrophysiological (including the following optical mapping) studies. Consistent with our previous report,²⁰ the compound KO mice had significantly lower body weight compared with the WT mice (23.4 ± 4.1 g versus 28.4 ± 5.8 g, $P = 0.03$). The mean dry heart weight was 0.22 ± 0.04 g (DM mutant) versus 0.20 ± 0.04 g (WT) ($P = 0.27$). As a result, DM mutant mice had a significantly higher heart weight/body weight ratio than the WT mice (0.95% versus 0.71%, $P < 0.001$).

Ultrastructural Analysis of DM Mutant Mice Revealed Morphological Defects Similar to Clinical DM Hearts

The DM mutant mice remained the same phenotypes of enhanced myotonia, muscular weakness, and sudden death after transferring from Gainesville, Florida (USA), to Keelung, Taiwan. To further investigate the ultrastructural abnormalities of KO hearts, we performed transmission electron microscopy studies on 3 pairs of WT and DM mutant mice, respectively. In contrast to parallel and tightly bounded myofibrils in WT mice (Figure 1A), mutant mice showed disarrangement and overcontraction of myofibrils with extended side-to-side junctions. In addition, numerous enlarged mitochondria accompanied with vacuolar spaces were also observed (Figure 1B). The enclosed areas in Figure 1A and 1B were magnified and shown in Figure 1C (WT) and 1D (DM mutant). Unlike the WT mice that showed organized segment and distinct Z lines, the myofibrils in DM mutant mice were destructed and replaced with vacuoles. These results further confirmed that the DM mutant mice used in this study possess typical DM cardiac manifestations, and these findings may underlie cardiac abnormalities including arrhythmia in DM mouse hearts.

DM Mutant Mice Showed Spontaneous Arrhythmogeneity During Baseline Recordings

Before general anesthesia, 2 of 12 DM mutant mice were apneic and underwent cardiac arrest soon after premedication

of xylazine (10 mg/kg IP) and zoletil (25 mg/kg IP). The baseline ECG recordings revealed spontaneous episodes of incessant atrial tachycardia in nearly all (9 of 10) of the remaining mutant mice (Figure 2A-a). In addition, nearly a third (3 of 10) of the DM mutant mice showed high-grade atrioventricular block after intubation under general anesthesia (Figure 2A-b). In contrast, none of the WT mice showed atrial tachycardia or atrioventricular block during in vivo baseline recording ($P < 0.001$) (Figure 2B). Also, DM mutant mice had significantly longer PR intervals (44 ± 6 ms, $n = 10$) compared with the WT mice (38 ± 4 ms, $n = 14$) ($P = 0.014$) (Figure 2C).

Optical Mapping Analysis Revealed No Change of Calcium Dynamics in DM Mutant Mice

The DM mutant mice had a significantly longer ventricular effective refractory period than WT mice (49 ± 8 ms versus 39 ± 9 ms, $P = 0.015$) and longer APD_{80} at all PCLs than the WT mice (Figure 3A). In contrast, there was no significant difference of Ca_iTD_{80} at all PCLs between the 2 groups (Figure 4A). APD_{80} and Ca_iTD_{80} heterogeneity analyses showed no significant differences between the DM mutant and WT mice (Figures 3B and 4B). Representative recording of action potential and Ca_i tracings from the same heart are shown in Figures 3C and 4C. The Ca_i tracings and Ca_iTD_{80} maps show similar Ca_iTD_{80} between the 2 hearts. In addition to Ca_i transient duration, the τ values of Ca_i decay also showed no difference (WT 34 ± 3 ms versus DM mutant 33 ± 2 ms; $P = 0.26$). The discrepancy of longer APD_{80} with similar Ca_iTD_{80} and Ca_i decay suggests that other ionic mechanisms, rather than Ca_i dynamic, may account for the APD_{80} prolongation in the DM mutant mice.

Slowing of CV in DM Mutant Mice

The DM mutant mice displayed significantly slower CV compared with the WT mice (Figure 5A). A representative example of isochronal maps obtained by dynamic pacing in both groups was shown in Figure 5B. Upon the stimulation with a series of PCLs at 200, 150, 120, 100, 90, 80, and 70 ms, the CVs measured both from the pacing site to left ventricular apex or the pacing site along atrioventricular ring were both significantly reduced. To describe the values in Figure 5B more specifically, the former CVs were 83, 76, 69, 69, 64, 59, and 52 cm/s in this particular WT mouse and 55, 51, 51, 48, 48, 43 and 42 cm/s in this particular DM mutant mouse and the latter were 88, 88, 77, 77, 77, 77, and 77 cm/s in this particular WT mouse and 59, 59, 53, 53, 48, 48, 41 cm/s in this DM mutant mouse, respectively. Note that functional conduction block was only induced in the DM mutant hearts (at

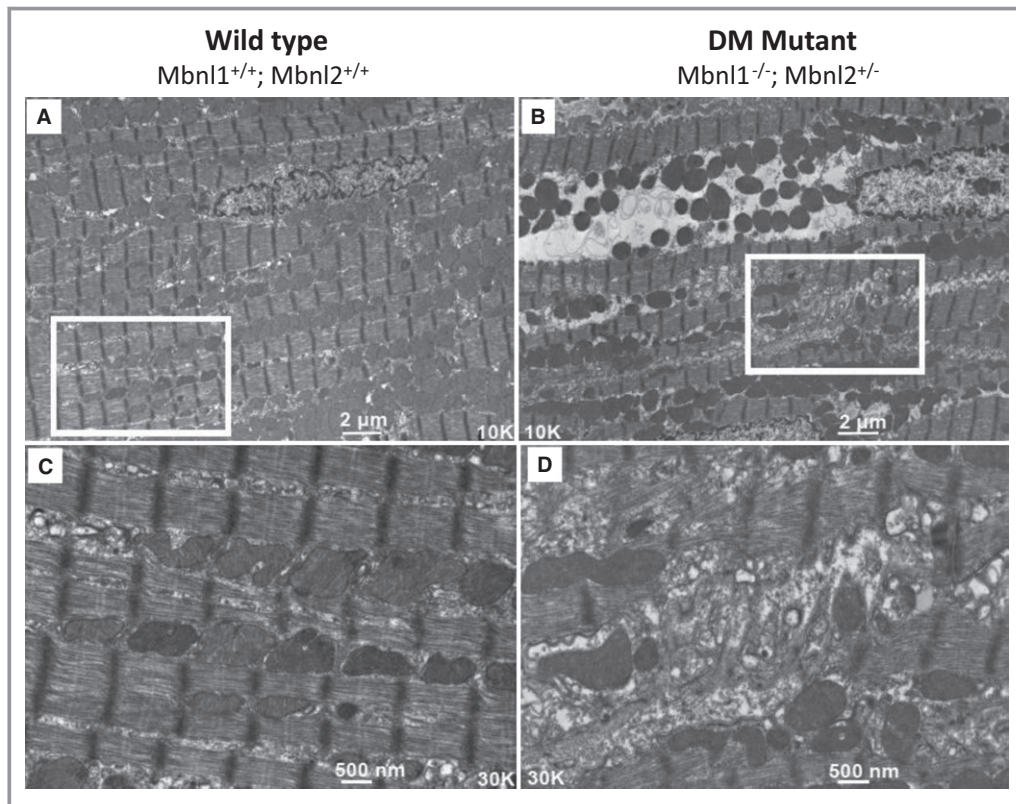


Figure 1. Electromicroscopic investigations of cardiac muscle of wild-type (WT) and dystrophia myotonica (DM) mutant mice. A, WT cardiac muscle showed well-organized fiber orientation and orderly aligned muscular segments ($\times 10K$). B, DM mutant mice myocardium showed muscle fiber disarrangement and disordered muscular segments. The muscle fibers were separated by interspace packed with vacuoles and enlarged mitochondria, indicating a degenerating process ($\times 10K$). C, Enclosed image from figure (A) showed parallel arrangement of continuous myofibrils and organized microstructural lines in between actin and myosin fibers ($\times 30K$). D, Enclosed image from figure (B) showed disrupted myofibrils from a DM mutant mouse ($\times 30K$). Mbnl indicates muscleblind-like.

a PCL of 70 ms, subpanel at right lower corner of Figure 5B), which could have perpetuated reentry formation and ventricular tachyarrhythmias.

DM Mutant Mice Showed Steeper CV Restitution Curve Slopes

APD restitution analyses showed no significant difference of APD restitution curve slope between the WT mice and DM mutant mice (1.125 ± 0.172 versus 1.245 ± 0.240 ; $P=0.103$ [Figure 6A]). Figure 6B shows representative APD restitution curves of a WT mouse and a DM mutant mouse. The DM mutant mice had significantly steeper slopes in CV restitution curves than the WT mice (Figure 6C). The slopes of CV restitution curves in WT versus DM mutant mice were 0.479 ± 0.142 cm/s per ms versus 0.675 ± 0.195 cm/s per ms and 0.478 ± 0.145 cm/s per ms versus 0.654 ± 0.137 cm/s per ms from the left ventricular lateral wall pacing site along the atrioventricular ring and to the left ventricular apex, respectively. Figure 6D shows representative

CV restitution curves of a WT mouse and a DM mutant mouse.

The Induction of SDA was a Common Feature in *Mbnl* Compound KO Mice That Increased Susceptibility of Conduction Block

The spatially concordant V_m and Ca_i alternans could be induced simultaneously in all mice by decremental pacing in both groups, and there was no significant difference of the longest PCL to induce spatially concordant alternans (SCA) between the WT (94 ± 10 ms) and DM mutant mice (98 ± 14 ms, $P=0.54$). However, the DM mutant hearts showed a higher risk of SDA compared with the WT hearts: the SDA was more easily inducible in mutant (8 of 10, 80%) than WT mice (5 of 14, 36%; $P=0.036$). The longest PCL to induce SDA in DM mutant hearts was 79 ± 6 ms, slightly longer than WT (70 ± 10 ms, $P=0.078$). An example of SDA induction is shown in Figure 7. Progressive shortening of PCL to 80 ms induced SCA (Figure 7A, left panels). When PCL was

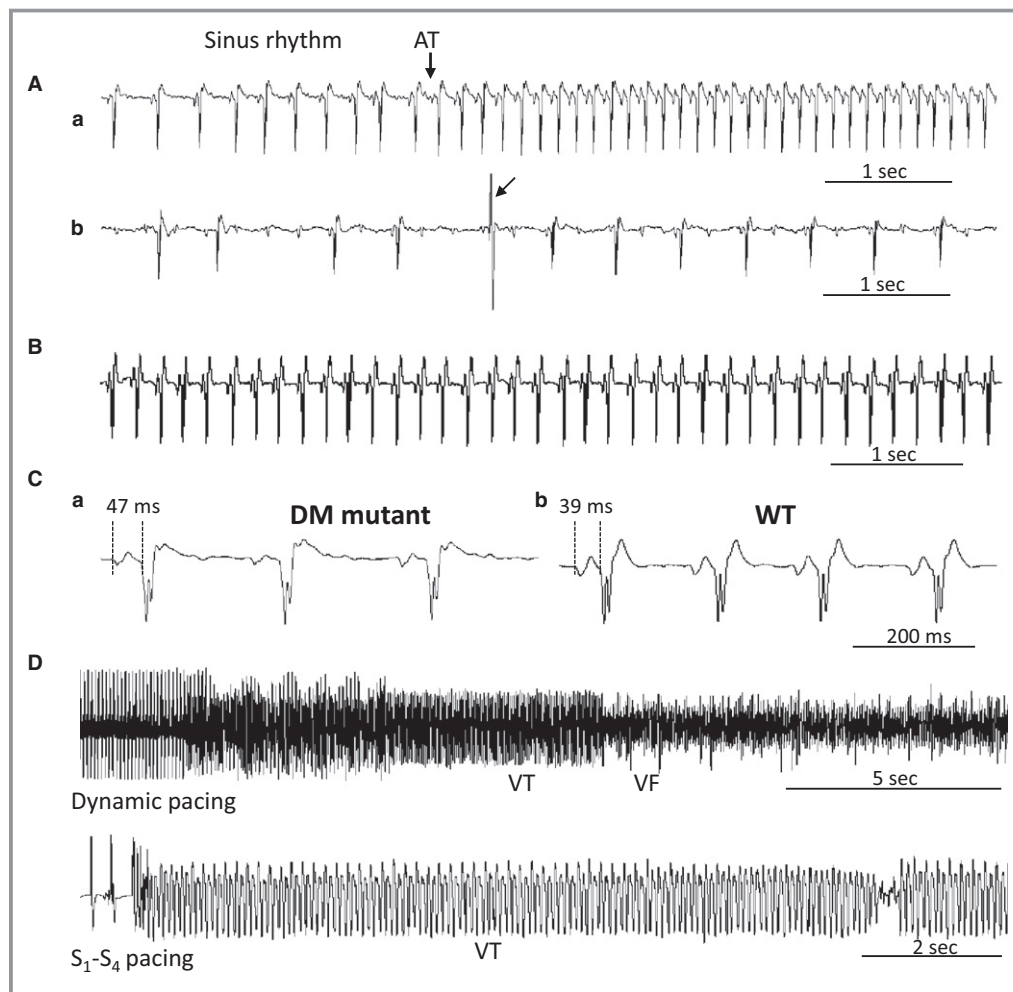


Figure 2. ECG recordings. A, Representative example of dystrophin myotonic (DM) mutant mice showing (a) sudden onset of atrial tachycardia (AT) from a regular sinus rhythm (SR) and (b) high-grade atrioventricular (AV) block and ventricular premature beats (arrow). B, Normal SR recorded from a wild-type (WT) mouse. C, The ECG tracings from a DM mutant (a) and a WT (b) heart showing a prolonged PR interval in mutant (47 ms) compared with WT (39 ms) mouse, evidence of first-degree AV block. D, Ventricular tachycardias induced by 2 different pacing protocols (dynamic and S₁-S₄) in a DM mutant heart. VF indicates ventricular fibrillation; VT, ventricular tachycardia.

further shortened to 70 ms, the SDA (Figure 7A, middle and right panels, and Figure 7C, left panel) was induced and the mapping field was separated by 2 nodal lines (arrows in Figure 7A, middle panel). These lines moved farther towards the pacing site at a shorter PCL of 60 ms. Note that V_m and Ca_i transients were out of phase in different regions of the heart during the SDA, which resulted in a dispersion of refractoriness and increased the susceptibility to functional conduction block.

The DM Mutant Mice are Predisposed to VT/VF Induction

The DM mutant mice were more susceptible to the induction of ventricular tachycardia. The inducibility of VT/VF was

9 of 10 (90%) in DM mutant mice and 5 of 14 (36%) in WT mice ($P=0.011$), and the sustainability of VT/VF were also significantly higher in mutant (7 of 10 [70%]), compared with WT (1 of 14 [7%]; $P=0.002$). A representative example of pseudo-ECG findings of VT/VF induction was shown in Figure 2D. Both dynamic pacing and S₁-S₄ (300-60-60-50 ms) pacing could induce sustained ventricular tachycardia in DM mutant hearts.

The possible causal relationship between SDA and ventricular tachycardia induction during dynamic pacing are illustrated in Figure 7. The pseudo-ECG (Figure 7C, right upper panel) and V_m (Figure 7C, lower panel) recordings are shown simultaneously, and a fragmented V_m tracing was found at site “a” (located on the nodal line labeled in Figure 7B), at the initiation of ventricular tachycardia (red

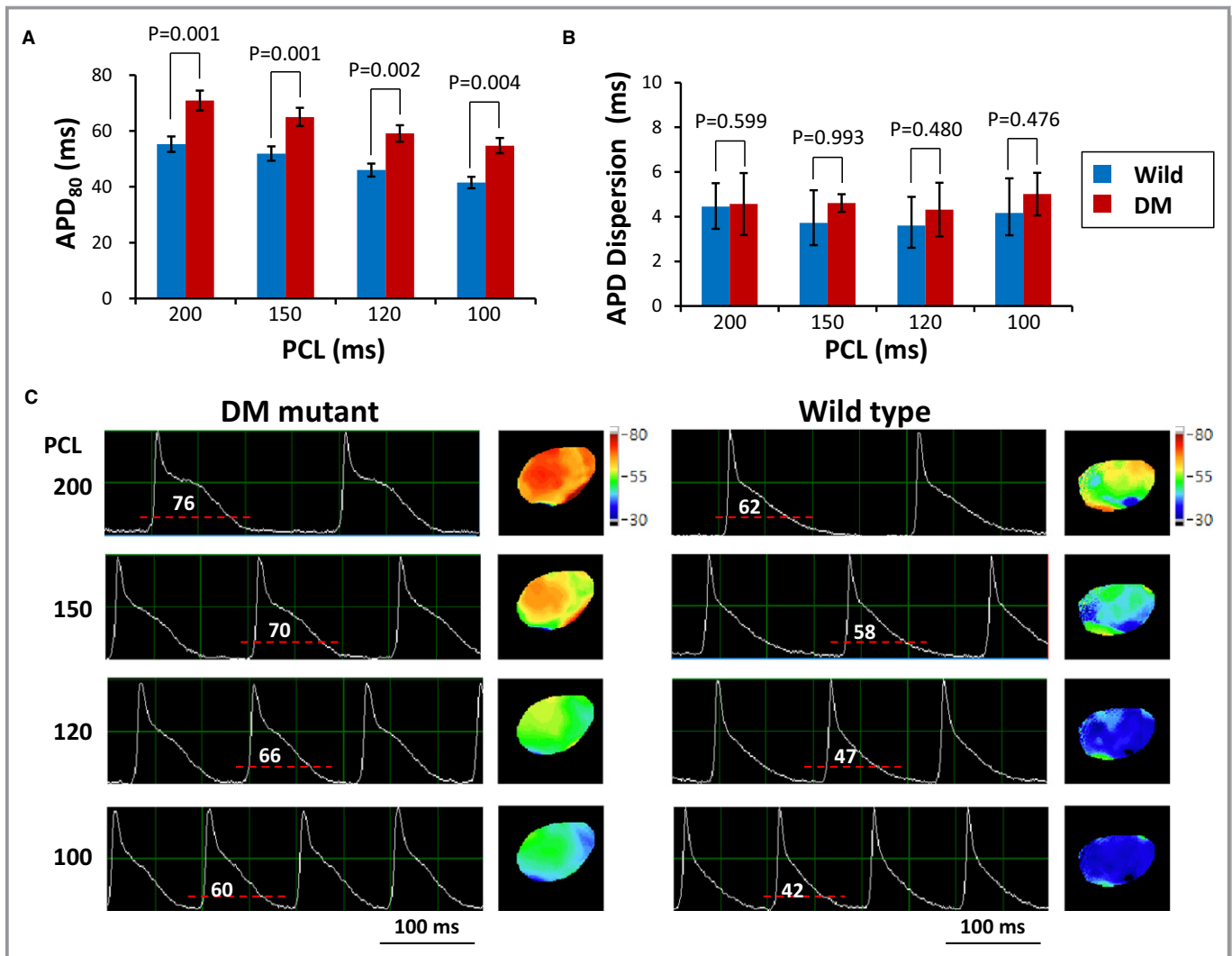


Figure 3. Prolongation of action potential duration (APD) in dystrophia myotonica (DM) mutant mice. A, Mean value of the APD measured from 20% depolarization to 80% repolarization (APD_{80}) vs pacing cycle length (PCL) for wild-type (WT) ($n=9$) and DM mutant ($n=12$) hearts. B, Bar graph showing statistical summary of APD dispersion in WT ($n=8$) and DM mutant ($n=12$) mice. C, Optical membrane voltage (V_m) tracings and APD_{80} maps at a pacing cycle length (PCL) of 200, 150, 120, and 100 ms in both groups.

arrow in Figure 7C, lower panel a). The simultaneously recorded isochronal maps, corresponding to the short run ECG reading (labeled as the red bar) in Figure 7C (lower panel b), is shown in Figure 7D. The CV alternans occurred while the PCL was shortened to 50 ms (fast and slow CV at frames 75 and 125 ms, respectively). The functional conduction block (frame 175 ms) followed to generate reentrant wave fronts that eventually lead to sustained ventricular tachyarrhythmia (Video S1).

Immunoblotting of $Na_v1.5$ Protein

To verify factors that may change the regulation of sodium current, we chose to analyze the expression level of the $Na_v1.5$ (*Scn5a*) protein by immunoblotting. Previously, the

mis-splicing of *SCN5A* without affecting mRNA level has been reported in a DM patient study.²³ Our normalized Western blot results showed no significant changes of $Na_v1.5$ protein level between WT and DM mutant mice, which is compatible with the results seen in patients (Figure 8; $n=4$ in each group, $P=0.564$).

Discussion

Cardiac manifestations are commonly seen in a variety of hereditary muscular dystrophies. Similar to other inherited muscular dystrophies, the cardiac manifestations in DM may come after skeletal muscular symptoms or they could be the presenting features. Compared with Duchenne muscular dystrophy, ventricular dysfunction and heart failure are much

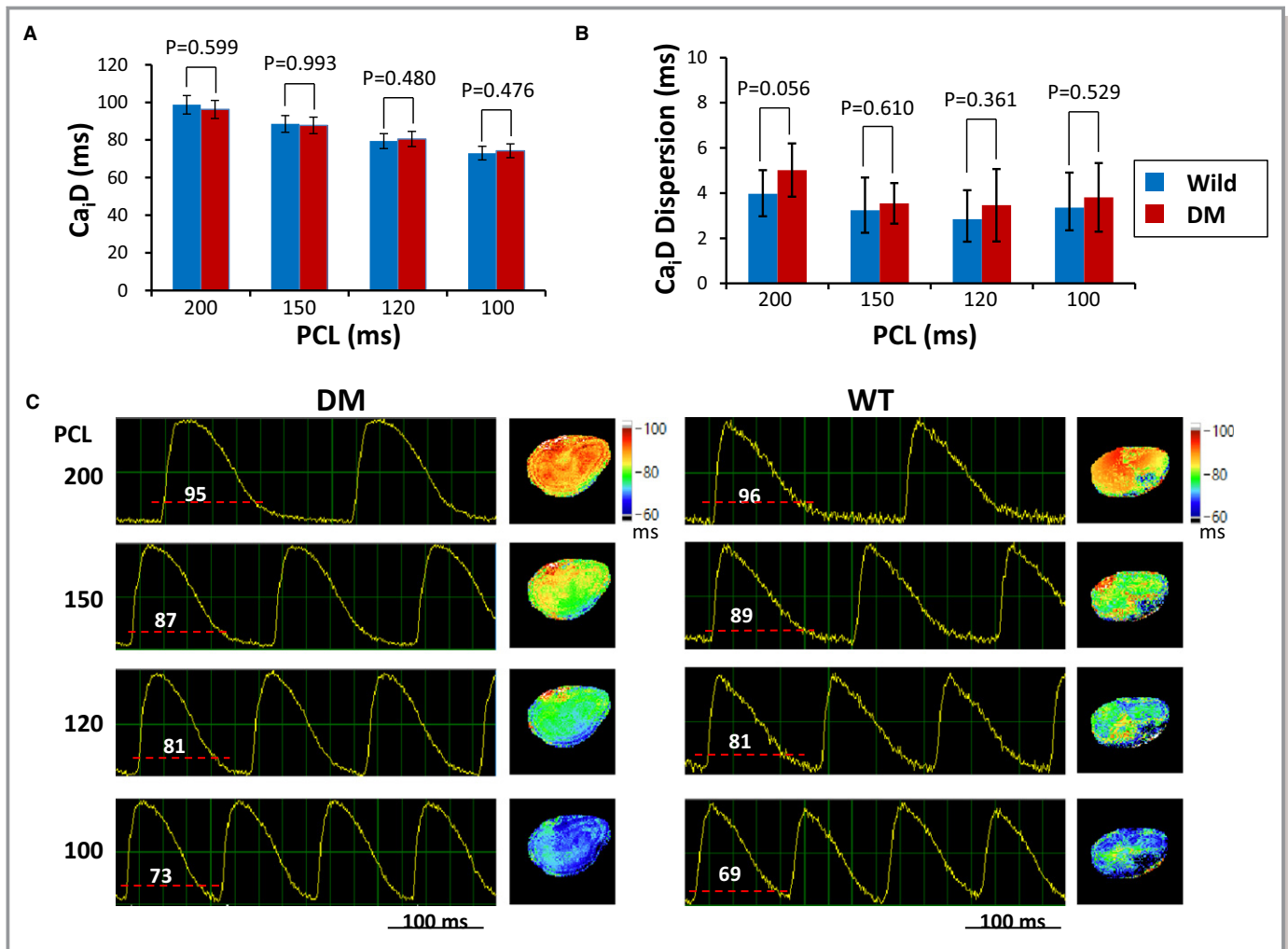


Figure 4. No significant differences in the intracellular calcium (Ca_i) transient duration ($\text{Ca}_i\text{TD}_{80}$) between wild-type (WT) and dystrophia myotonica (DM) mutant mice. A, Bar graph showing statistical summary of $\text{Ca}_i\text{TD}_{80}$ in WT ($n=8$) and DM mutant ($n=12$) mice. B, Bar graph showing statistical summary of Ca_iTD dispersion in WT ($n=8$) and DM mutant ($n=12$) mice. C, Optical Ca_i tracings and $\text{Ca}_i\text{TD}_{80}$ maps at a pacing cycle length (PCL) of 200, 150, 120, and 100 ms.

less common and only seen in end-stage DM patients.²⁴ The incidence of arrhythmia-related sudden death is higher in DM1 patients. However, DM type II patients are also at risk for severe cardiac complications.^{13,25} Pathological studies on DM patient heart samples revealed myocardial degeneration, fatty infiltration, or diffuse or focal fibrosis throughout myocardium or limited to the conduction system.^{26,27} Electron microscopic studies showed disarray of myofibrils, defective mitochondrial morphology, indistinct Z lines, and numerous vacuoles.^{28–30} These features could also be seen in our *Mbnl* compound KO mice. The myofibril disarray may contribute to the cardiac presentations in DM patients, and fibrosis may serve as a substrate for reentrant arrhythmia.^{31,32}

Conduction block–related asystole or ventricular tachyarrhythmia may contribute to sudden death, and the latter may be more common in DM patients than expected.^{3,7} To

determine the mechanisms of ventricular tachyarrhythmias in DM, Merino et al³³ performed invasive electrophysiological studies and concluded that bundle branch reentry accounts for the tachycardia. For these patients who had inducible ventricular tachyarrhythmias, they recommended radiofrequency catheter ablation as an effective intervention. In addition to conduction block, CV restitution and fixed electrophysiological heterogeneity of myocardium also contribute to the development of SDA.^{34,35} Rapid heart rate and ectopic beats further enhance initiation of SDA, reentry, and development of arrhythmias.³⁴ In our study, we performed simultaneous V_m and Ca_i optical mapping to investigate whether abnormal Ca_i dynamic plays a role in ventricular arrhythmogenesis. As shown in our mapping data, the differences of $\text{Ca}_i\text{TD}_{80}$, Ca_i decay, and threshold of Ca_i alternans between mutant and WT hearts were insignificant. However, it is interesting that mutant hearts had significantly slower CV, steeper slope of CV restitution curve,

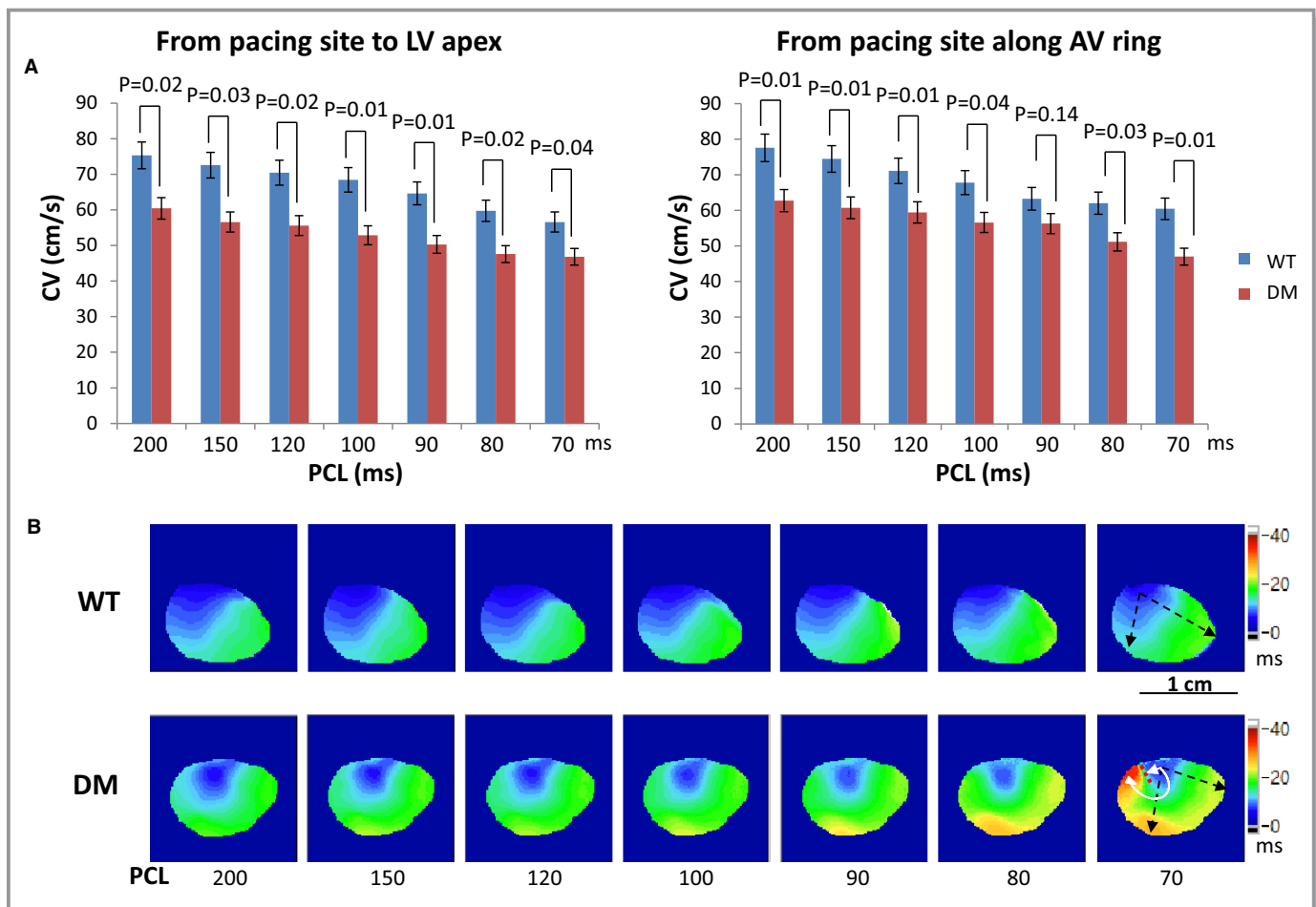


Figure 5. Reduced conduction velocity (CV) in dystrophia myotonica (DM) mutant mice. A, Summary of CV measured from the pacing site to left ventricular (LV) apex (left) and along the atrioventricular (AV) ring (right) in wild-type (WT) (n=8) and DM mutant (n=11) mice. B, Isochronal maps at a pacing cycle length (PCL) from 200 to 70 ms. The black arrows indicate the directions of CV measurement, the white arrows indicate wave fronts propagation, and the red dot line indicates functional conduction block at a PCL of 70 ms.

and higher susceptibility to SDA induction, which also facilitated SDA development, reentry formation, and ventricular fibrillation induction.³⁴ As shown in Figures 5 and 6, rate-dependent conduction delay prolonged the time differences in depolarization between myocytes, thereby raising spatial gradients of activation and perpetuating the onset of arrhythmogenic SDA.³⁶ When CV was reduced sufficiently for regaining excitability of the myocardial tissue ahead of the excitation wave front, reentrant circuits were formed and self-generating. However, whether the reentry hypothesis could also be applied to polymorphic ventricular tachycardia, which is occasionally seen in DM patients, needs further investigation.¹³

From the molecular perspective, DM has a unique underlying mechanism supported by evidence from various mouse models.^{37–40} Instead of perturbing the expression of the genes (eg, DM protein kinase), the pathogenic effects of extended microsatellite repeats are mediated through the hairpin structure formed by the transcribed (CC(U)G)_n RNA. These double-stranded hairpins interact with a variety of RNA-

binding proteins to form RNA foci and retain in the nuclei. Confocal images revealed these foci are only “colocalizing” with MBNL proteins, but not other RNA-binding proteins.⁴¹ Although a variety of disease mechanisms have been suggested, potentially generated by the extended repeats (eg, repeat associated non-ATG (RAN) translation),⁴² we hypothesized that the primary events in the RNA-dominant model is the MBNL loss of function and proved with a series of *Mbnl* KO mouse models. Various transgenic mouse models expressing pathogenic repeats in specific tissues are available; however, mice simultaneously presenting myotonia and corresponding cardiac defects are extremely rare. Since myotonia is the hallmark symptom of DM, it is ideal for a DM mouse model to show this typical phenotype as a reliable control. To our knowledge, this is the first cardiac optical mapping study on DM mouse models and importantly, the *Mbnl1*^{-/-}; *Mbnl2*^{+/-} mice with robust myotonia.

Although various MBNL-misregulated genes are related to calcium homeostasis or sensitive to calcium level (eg, *Cacna1s*,

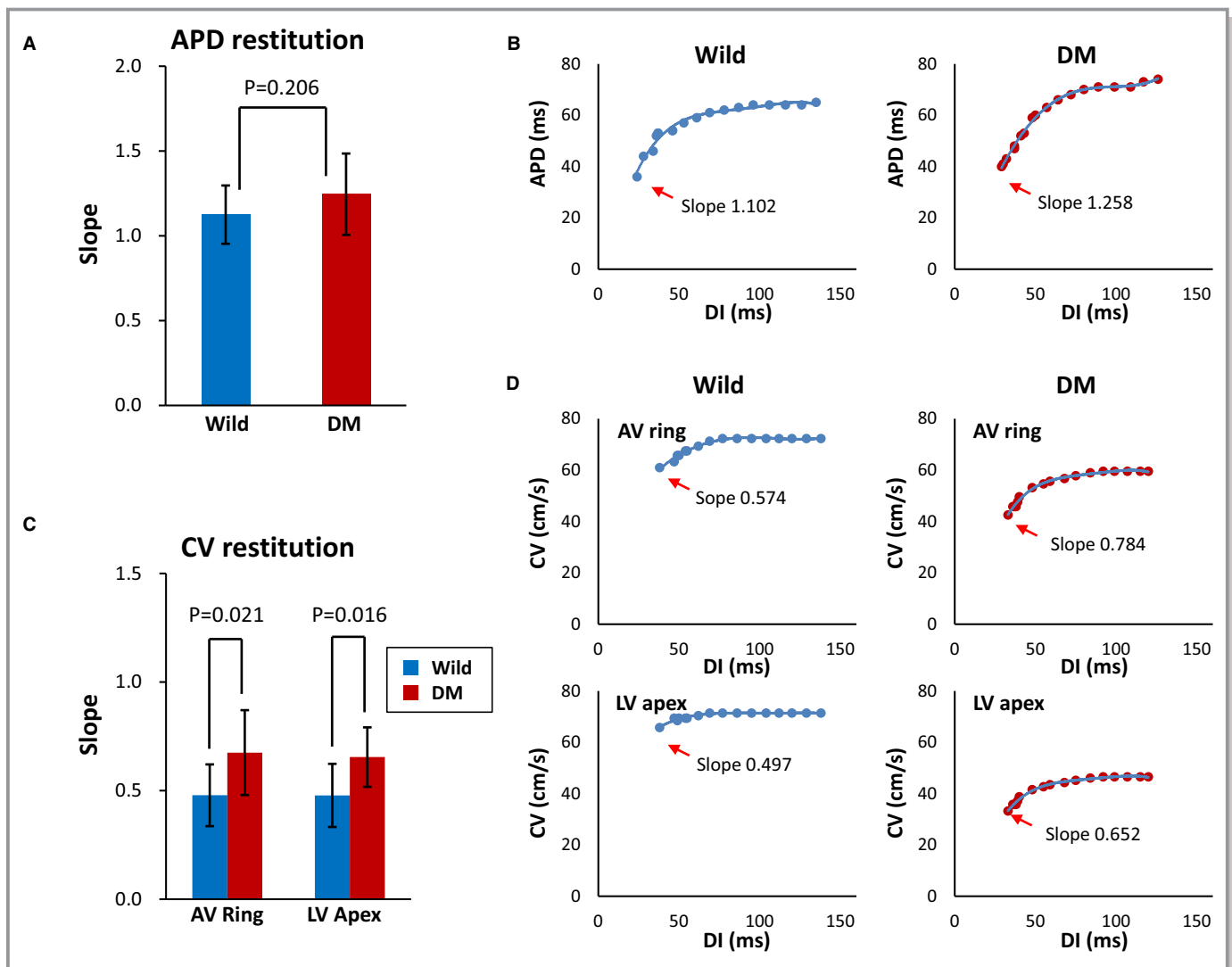


Figure 6. Action potential duration (APD) and conduction velocity (CV) restitution curves. A, APD restitution slope of the wild-type (WT) (n=8) and the dystrophia myotonica (DM) mutant mice (n=12). B, Representative APD restitution curves of a WT mouse and a DM mutant mouse. C, CV restitution slope of the WT (n=8) and the DM mutant (n=11) mice. D, Representative CV restitution curves of a WT mouse and a DM mutant mouse.

Tnnt2), several reports instead highlight the importance of sodium channel misregulation in DM arrhythmogenicity. In a study by Freyermuth et al,²³ inclusion of the exon 6A of SCN5A (the gene that encodes Na_v1.5 sodium channel) was increased in DM heart samples as well as in *Mbn1* KO; *Mbn2* HET mice. Through a series of electrophysiological analysis on different isoforms they concluded that the misregulation of SCN5A splicing accounts for DM arrhythmia.²³ In concordance with this report, Wahbi et al⁴³ also reported that Brugada syndrome may cause cardiac sudden death in DM patients and SCN5a mis-splicing may play a role. Also, Pambrun et al⁴⁴ reported that patients carrying the DM1 mutant allele from the paternal side could have exacerbated Brugada syndrome induced by sodium channel mutation coming from the maternal side. In addition to misregulation of SCN5A splicing, other DM animal

models showed abnormal sodium channel gating.^{45,46} Slow decay of sodium currents, late reopenings of sodium channels, and relatively depolarized resting membrane potential contribute to prolonged action potential in DM cardiomyocytes.⁴⁵ It seems that exploring the dynamic nature of I_{Na} is promising for an integrated understanding of the mechanisms, which may directly link I_{Na} dysfunction to DM cardiac pathophysiology.

Limitations

There are several limitations in this study. Although the phenotypic presentations are similar to clinical DM, the features of cardiac arrhythmias in this DM animal model might not be identical to arrhythmias in patients. Small and large animals have different expressions of calcium handling

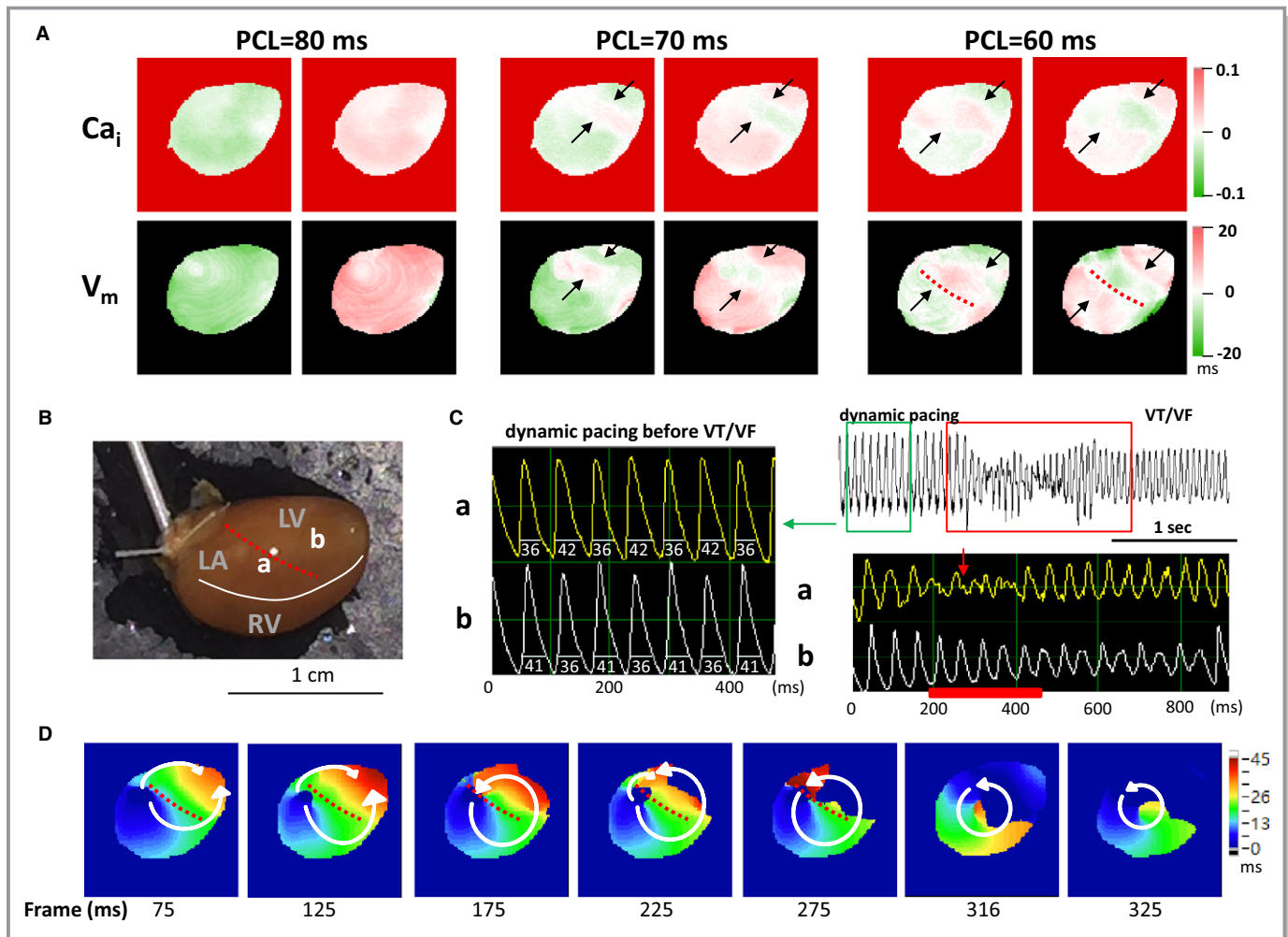


Figure 7. Pacing-induced spatially discordant alternans (SDA) and ventricular tachyarrhythmia in dystrophia myotonica (DM) mutant mice. **A**, Membrane voltage (V_m) and intracellular calcium (Ca_i) alternans maps. Concordant alternans was induced at a pacing cycle length (PCL) of 80 ms, and proceeded to SDA by a shorter PCL (70 ms). The black arrows indicate nodal lines. **B**, Mapping field. **C**, Pseudo-ECG (top subpanel) and the corresponding V_m tracings recorded at site (a and b) in the mapping field (left and bottom subpanels). The green square shows the pseudo-ECG tracing of corresponding V_m tracings (left subpanel) of SDA development during dynamic pacing immediately before development of ventricular tachycardia/ventricular fibrillation (VT/VF); the numbers represent the action potential duration measured from 20% depolarization to 80% repolarization (APD_{80}) of the particular beats. The red square indicates ventricular tachyarrhythmia initiation. **D**, Isochronal maps. The numbers below each frame are the time points (ms) after the start of data acquisition from time zero. The white arrows indicate the directions of wave fronts propagation, and the red dot lines indicate functional conduction block, corresponding to a nodal line. LA indicates left atrium; LV, left ventricle; RV, right ventricle.

proteins and ion channels,⁴⁷ leading to different action potential morphology and cardiac electrophysiology. This is still an observational study and characterization of an animal model rather than data from clinical patients, and therefore further investigation is required for clinically relevant mechanisms. Excitation-contraction uncouplers are required to suppress motion artifacts in optical mapping studies, but these agents have significant electrophysiological effects, including APD prolongation, effective refractory period increase, and restitution curve alteration.^{48,49} The electrophysiological presentations in optical mapping studies might be different from that in vivo. Ultrastructural analyses from transmission electron

microscopy showed enlarged mitochondria with vacuole formation, and the changes may play a role in reduced cardiac contraction. It has been shown that DM protein kinase protects cells and mitochondria from oxidative stress and cell death in a DM1 mouse model.⁵⁰ However, whether mitochondrion dysfunction directly influences cardiac conduction or calcium handling in our model needs further evaluation.

Conclusions

We confirmed that severe cardiac arrhythmias could develop in the *Mbnl* compound KO mice and that sudden death in this

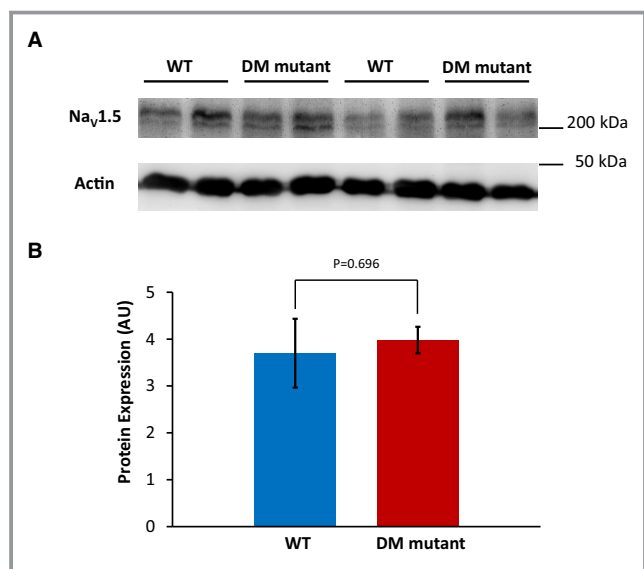


Figure 8. Immunoblotting of $\text{Na}_v1.5$ protein. A, Western blotting analysis of $\text{Na}_v1.5$ (Scn5a) in wild-type (WT) and dystrophia myotonica (DM) mutant mouse heart tissues. B, Quantitative analysis of protein expression. The normalized level of Scn5a protein in the hearts of DM mutant mice did not show significant changes, compared with WT mice ($n=4$ in each group, $P=0.564$). AU indicates arbitrary unit.

mouse line is reasonably cardiogenic. This lethal phenomenon was caused by a significantly slower CV that contributed to higher susceptibility of conduction disturbance and SDA. Since mutant mice have longer APD_{80} but no difference in $\text{Ca}_i\text{TD}_{80}$ and Ca_i decay τ values compared with WT, ionic mechanisms other than Ca^{2+} may be involved in ventricular tachyarrhythmias in DM patients. These findings are highly compatible with current knowledge about DM arrhythmogenesis and may imply an I_{Na} dysfunction-based mechanism of ventricular tachyarrhythmias. Clinically, since rapid ventricular rate may increase the risk of ventricular tachyarrhythmias in DM patients, cautious heart rate control with conduction system monitoring is indicated. Implantable cardioverter-defibrillator and/or radiofrequency ablation rather than antiarrhythmic agents for tachyarrhythmias seems to be a suitable strategy based on the evidence of reduced CV and susceptibility to SDA induction observed in this DM mouse model.

Acknowledgments

The authors thank Dr Maurice Swanson, the professor in the Department of Molecular Genetics and Microbiology and the Center for NeuroGenetics, University of Florida, College of Medicine, for the generous agreement of transferring *Mbnl1* and *Mbnl2* KO mouse lines. The transmission electron microscopy studies were facilitated by the Microscope Core Laboratory, Chang Gung Memorial Hospital, Linkou, Taiwan. The authors also thank Carol

Seah for her contributions on mouse husbandry and immunoblotting analyses.

Sources of Funding

This work was supported by Chang Gung Medical Research Grant, Keelung (CMRPG2D0181 and CMRPG2F0281 to Lee) and Linkou (CMRPG3F035 to Chou; CMRPG3D034 to Chang).

Disclosures

None.

References

1. Fu YH, Pizzuti A, Fenwick RG Jr, King J, Rajnarayan S, Dunne PW, Dubel J, Nasser GA, Ashizawa T, de Jong P, Wieringa B, Korneluk R, Perryman MB, Epstein HF, Thomas Caskey C. An unstable triplet repeat in a gene related to myotonic muscular dystrophy. *Science*. 1992;255:1256–1258.
2. Liquori CL, Ricker K, Moseley ML, Jacobsen JF, Kress W, Naylor SL, Day JW, Ranum LP. Myotonic dystrophy type 2 caused by a CCTG expansion in intron 1 of ZNF9. *Science*. 2001;293:864–867.
3. Nigro G, Papa AA, Politano L. The heart and cardiac pacing in steinert disease. *Acta Myol*. 2012;31:110–116.
4. Mathieu J, Allard P, Potvin L, Prevost C, Begin P. A 10-year study of mortality in a cohort of patients with myotonic dystrophy. *Neurology*. 1999;52:1658–1662.
5. Clarke NR, Kelion AD, Nixon J, Hilton-Jones D, Forfar JC. Does cytosine-thymine-guanine (CTG) expansion size predict cardiac events and electrocardiographic progression in myotonic dystrophy? *Heart*. 2001;86:411–416.
6. Groh WJ, Lowe MR, Zipes DP. Severity of cardiac conduction involvement and arrhythmias in myotonic dystrophy type 1 correlates with age and CTG repeat length. *J Cardiovasc Electrophysiol*. 2002;13:444–448.
7. Groh WJ, Groh MR, Saha C, Kincaid JC, Simmons Z, Ciafaloni E, Pourmand R, Otten RF, Bhakta D, Nair GV, Marashdeh MM, Zipes DP, Pascuzzi RM. Electrocardiographic abnormalities and sudden death in myotonic dystrophy type 1. *N Engl J Med*. 2008;358:2688–2697.
8. Collier JA, Hawley RJ, Pinnow EE, Kokkinos PF, Fletcher RD. Value of the electrocardiogram in determining cardiac events and mortality in myotonic dystrophy. *Am J Cardiol*. 1997;80:1494–1497.
9. Bassez G, Lazarus A, Desguerre I, Varin J, Laforet P, Becane HM, Meune C, Arne-Bes MC, Ounnoughene Z, Radvanyi H, Eymard B, Duboc D. Severe cardiac arrhythmias in young patients with myotonic dystrophy type 1. *Neurology*. 2004;63:1939–1941.
10. Laurent V, Pellioux S, Corcia P, Magro P, Pierre B, Fauchier L, Raynaud M, Babuty D. Mortality in myotonic dystrophy patients in the area of prophylactic pacing devices. *Int J Cardiol*. 2011;150:54–58.
11. Pelargonio G, Dello Russo A, Sanna T, De Martino G, Bellocci F. Myotonic dystrophy and the heart. *Heart*. 2002;88:665–670.
12. Bhakta D, Shen C, Kron J, Epstein AE, Pascuzzi RM, Groh WJ. Pacemaker and implantable cardioverter-defibrillator use in a US myotonic dystrophy type 1 population. *J Cardiovasc Electrophysiol*. 2011;22:1369–1375.
13. Benhayon D, Lugo R, Patel R, Carballeira L, Elman L, Cooper JM. Long-term arrhythmia follow-up of patients with myotonic dystrophy. *J Cardiovasc Electrophysiol*. 2015;26:305–310.
14. Pascual M, Vicente M, Monferrer L, Artero R. The muscleblind family of proteins: an emerging class of regulators of developmentally programmed alternative splicing. *Differentiation*. 2006;74:65–80.
15. O'Rourke JR, Swanson MS. Mechanisms of RNA-mediated disease. *J Biol Chem*. 2009;284:7419–7423.
16. Batra R, Charizanis K, Manchanda M, Mohan A, Li M, Finn DJ, Goodwin M, Zhang C, Sobczak K, Thornton CA, Swanson MS. Loss of MBNL leads to disruption of developmentally regulated alternative polyadenylation in RNA-mediated disease. *Mol Cell*. 2014;56:311–322.
17. Goodwin M, Mohan A, Batra R, Lee KY, Charizanis K, Gomez FJ, Eddarkaoui S, Sergeant N, Buee L, Kimura T, Clark HB, Dalton J, Takamura K, Weyn-Vanhenyryck SM, Zhang C, Reid T, Ranum LP, Day JW, Swanson MS. MBNL sequestration by toxic RNAs and RNA misprocessing in the myotonic dystrophy brain. *Cell Rep*. 2015;12:1159–1168.

18. Kanadia RN, Johnstone KA, Mankodi A, Lungu C, Thornton CA, Esson D, Timmers AM, Hauswirth WW, Swanson MS. A muscleblind knockout model for myotonic dystrophy. *Science*. 2003;302:1978–1980.
19. Charizanis K, Lee KY, Batra R, Goodwin M, Zhang C, Yuan Y, Shiue L, Cline M, Scotti MM, Xia G, Kumar A, Ashizawa T, Clark HB, Kimura T, Takahashi MP, Fujimura H, Jinnai K, Yoshikawa H, Gomes-Pereira M, Gourdon G, Sakai N, Nishino S, Foster TC, Ares M Jr, Darnell RB, Swanson MS. Muscleblind-like 2-mediated alternative splicing in the developing brain and dysregulation in myotonic dystrophy. *Neuron*. 2012;75:437–450.
20. Lee KY, Li M, Manchanda M, Batra R, Charizanis K, Mohan A, Warren SA, Chamberlain CM, Finn D, Hong H, Ashraf H, Kasahara H, Ranum LP, Swanson MS. Compound loss of muscleblind-like function in myotonic dystrophy. *EMBO Mol Med*. 2013;5:1887–1900.
21. Chou CC, Wen MS, Lee HL, Chang PC, Wo HT, Yeh SJ, Wu D. Dantrolene suppresses ventricular ectopy and arrhythmogenicity with acute myocardial infarction in a langendorff-perfused pacing-induced heart failure rabbit model. *J Cardiovasc Electrophysiol*. 2014;25:431–439.
22. Chou CC, Zhou S, Miyauchi Y, Pak HN, Okuyama Y, Fishbein MC, Karagueuzian HS, Chen PS. Effects of procainamide on electrical activity in thoracic veins and atria in canine model of sustained atrial fibrillation. *Am J Physiol Heart Circ Physiol*. 2004;286:H1936–H1945.
23. Freyermuth F, Rau F, Kokunai Y, Linke T, Sellier C, Nakamori M, Kino Y, Arandel L, Jollet A, Thibault C, Philipps M, Vicaire S, Jost B, Udd B, Day JW, Duboc D, Wahbi K, Matsumura T, Fujimura H, Mochizuki H, Deryckere F, Kimura T, Nukina N, Ishiura S, Lacroix V, Campan-Fournier A, Navratil V, Chautard E, Auboeuf D, Horie M, Imoto K, Lee KY, Swanson MS, Lopez de Munain A, Inada S, Itoh H, Nakazawa K, Ashihara T, Wang E, Zimmer T, Furling D, Takahashi MP, Charlet-Berguerand N. Splicing misregulation of SCN5A contributes to cardiac-conduction delay and heart arrhythmia in myotonic dystrophy. *Nat Commun*. 2016;7:11067.
24. Hermans MC, Pinto YM, Merkies IS, de Die-Smulders CE, Crijns HJ, Faber CG. Hereditary muscular dystrophies and the heart. *Neuromuscul Disord*. 2010;20:479–492.
25. Schoser BG, Ricker K, Schneider-Gold C, Hengstenberg C, Durre J, Bultmann B, Kress W, Day JW, Ranum LP. Sudden cardiac death in myotonic dystrophy type 2. *Neurology*. 2004;63:2402–2404.
26. Nguyen HH, Wolfe JT III, Holmes DR Jr, Edwards WD. Pathology of the cardiac conduction system in myotonic dystrophy: a study of 12 cases. *J Am Coll Cardiol*. 1988;11:662–671.
27. Forsberg H, Olofsson BO, Eriksson A, Andersson S. Cardiac involvement in congenital myotonic dystrophy. *Br Heart J*. 1990;63:119–121.
28. Bulloch RT, Davis JL, Hara M. Dystrophia myotonica with heart block. A light and electron microscopic study. *Arch Pathol*. 1967;84:130–140.
29. Tanaka N, Tanaka H, Takeda M, Nimura T, Kanehisa T, Terashi S. Cardiomyopathy in myotonic dystrophy. A light and electron microscopic study of the myocardium. *Jpn Heart J*. 1973;14:202–212.
30. Harper PS. *Myotonic Dystrophy*. London, England: W.B. Saunders; 2001.
31. Turillazzi E, Neri M, Riezzo I, Di Paolo M, Evangelisti L, Fineschi V. Cardiac fibrosis, arrhythmia and sudden death in myotonic dystrophy type 1: could TGF- β 1 improve the predictive accuracy of patients at risk, opening new therapeutic challenges? *Int J Cardiol*. 2013;168:4976–4978.
32. Hermans MC, Faber CG, Bekkers SC, de Die-Smulders CE, Gerrits MM, Merkies IS, Snoep G, Pinto YM, Schalla S. Structural and functional cardiac changes in myotonic dystrophy type 1: a cardiovascular magnetic resonance study. *J Cardiovasc Magn Reson*. 2012;14:48.
33. Merino JL, Carmona JR, Fernandez-Lozano I, Peinado R, Basterra N, Sobrino JA. Mechanisms of sustained ventricular tachycardia in myotonic dystrophy: implications for catheter ablation. *Circulation*. 1998;98:541–546.
34. Weiss JN, Karma A, Shiferaw Y, Chen PS, Garfinkel A, Qu Z. From pulsus to pulseless: the saga of cardiac alternans. *Circ Res*. 2006;98:1244–1253.
35. Hayashi H, Shiferaw Y, Sato D, Nihei M, Lin SF, Chen PS, Garfinkel A, Weiss JN, Qu Z. Dynamic origin of spatially discordant alternans in cardiac tissue. *Biophys J*. 2007;92:448–460.
36. Watanabe MA, Fenton FH, Evans SJ, Hastings HM, Karma A. Mechanisms for discordant alternans. *J Cardiovasc Electrophysiol*. 2001;12:196–206.
37. Jansen G, Groenen PJ, Bachner D, Jap PH, Coerwinkel M, Oerlemans F, van den Broek W, Gohlsch B, Pette D, Plomp JJ, Molenaar PC, Nederhoff MG, van Echteld CJ, Dekker M, Berns A, Hameister H, Wieringa B. Abnormal myotonic dystrophy protein kinase levels produce only mild myopathy in mice. *Nat Genet*. 1996;13:316–324.
38. Mankodi A, Logigian E, Callahan L, McClain C, White R, Henderson D, Krym M, Thornton CA. Myotonic dystrophy in transgenic mice expressing an expanded CUG repeat. *Science*. 2000;289:1769–1773.
39. Wang GS, Kearney DL, De Biasi M, Taffet G, Cooper TA. Elevation of RNA-binding protein CUGBP1 is an early event in an inducible heart-specific mouse model of myotonic dystrophy. *J Clin Invest*. 2007;117:2802–2811.
40. Gomes-Pereira M, Foirey L, Nicole A, Huguet A, Junien C, Munnich A, Gourdon G. CTG trinucleotide repeat “big jumps”: large expansions, small mice. *PLoS Genet*. 2007;3:e52.
41. Fardaei M, Larkin K, Brook JD, Hamshire MG. In vivo co-localisation of MBNL protein with DMPK expanded-repeat transcripts. *Nucleic Acids Res*. 2001;29:2766–2771.
42. Cleary JD, Ranum LP. Repeat associated non-ATG (RAN) translation: new starts in microsatellite expansion disorders. *Curr Opin Genet Dev*. 2014;26:6–15.
43. Wahbi K, Algalarrondo V, Becane HM, Fressart V, Beldjord C, Azibi K, Lazarus A, Berber N, Radvanyi-Hoffman H, Stojkovic T, Behin A, Laforet P, Eymard B, Hatem S, Duboc D. Brugada syndrome and abnormal splicing of SCN5A in myotonic dystrophy type 1. *Arch Cardiovasc Dis*. 2013;106:635–643.
44. Pambrun T, Mercier A, Chatelier A, Patri S, Schott JJ, Le Scouarnec S, Chahine M, Degand B, Bois P. Myotonic dystrophy type 1 mimics and exacerbates Brugada phenotype induced by Nav1.5 sodium channel loss-of-function mutation. *Heart Rhythm*. 2014;11:1393–1400.
45. Lee HC, Patel MK, Mistry DJ, Wang Q, Reddy S, Moorman JR, Mounsey JP. Abnormal Na channel gating in murine cardiac myocytes deficient in myotonic dystrophy protein kinase. *Physiol Genomics*. 2003;12:147–157.
46. Reddy S, Mistry DJ, Wang QC, Geddis LM, Kutchai HC, Moorman JR, Mounsey JP. Effects of age and gene dose on skeletal muscle sodium channel gating in mice deficient in myotonic dystrophy protein kinase. *Muscle Nerve*. 2002;25:850–857.
47. Luss I, Boknik P, Jones LR, Kirchhefer U, Knapp J, Linck B, Luss H, Meissner A, Muller FU, Schmitz W, Vahlensieck U, Neumann J. Expression of cardiac calcium regulatory proteins in atrium v ventricle in different species. *J Mol Cell Cardiol*. 1999;31:1299–1314.
48. Brack KE, Narang R, Winter J, Ng GA. The mechanical uncoupler blebbistatin is associated with significant electrophysiological effects in the isolated rabbit heart. *Exp Physiol*. 2013;98:1009–1027.
49. Baker LC, Wolk R, Choi BR, Watkins S, Plan P, Shah A, Salama G. Effects of mechanical uncouplers, diacetyl monoxime, and cytochalasin-D on the electrophysiology of perfused mouse hearts. *Am J Physiol Heart Circ Physiol*. 2004;287:H1771–H1779.
50. Pantic B, Trevisan E, Citta A, Rigobello MP, Marin O, Bernardi P, Salvatori S, Rasola A. Myotonic dystrophy protein kinase (DMPK) prevents ROS-induced cell death by assembling a hexokinase II-Src complex on the mitochondrial surface. *Cell Death Dis*. 2013;4:e858.